


**Impact of biaxial and uniaxial strain on  $V_2O_3$** Darshana Wickramaratne<sup>1</sup>,<sup>✉</sup> Noam Bernstein,<sup>2</sup> and I. I. Mazin<sup>2,\*</sup><sup>1</sup>*NRC Research Associate, Resident at Center for Computational Materials Science, U.S. Naval Research Laboratory, Washington, DC 20375, USA*<sup>2</sup>*Center for Computational Materials Science, U.S. Naval Research Laboratory, Washington, DC 20375, USA* (Received 30 September 2019; revised manuscript received 4 November 2019; published 27 November 2019)

Using first-principles calculations, we determine the role of compressive and tensile uniaxial and equibiaxial strain on the structural, electronic, and magnetic properties of  $V_2O_3$ . We find that compressive strain increases the energy to transition from the high-temperature paramagnetic metallic phase to the low-temperature antiferromagnetic insulating phase. This shift in the energy difference can be explained by changes in the V-V bond lengths that are antiferromagnetically aligned in the low-temperature structure. The insights that we have obtained provide a microscopic explanation for the shifts in the metal-insulator transition temperature that have been observed in experiments of  $V_2O_3$  films grown on different substrates.

DOI: [10.1103/PhysRevB.100.205204](https://doi.org/10.1103/PhysRevB.100.205204)**I. INTRODUCTION**

The metal-to-insulator transition (MIT) in  $V_2O_3$  [1] has been the subject of intense investigations, due in part to the coupled structural, electronic, and magnetic phase transitions that occur in the material [2,3]. Above the bulk MIT temperature  $T_c$  of 155 K,  $V_2O_3$  is a metal and is stable in the corundum phase. Below  $T_c$ ,  $V_2O_3$  undergoes a structural transition from corundum to monoclinic. This is accompanied by the opening of a Mott gap of 0.40 eV below the MIT  $T_c$ , which manifests in a large increase in the electrical resistivity [4]. The co-occurrence of these phenomena has led to several efforts that have sought to control these phase transitions.

To understand and control the MIT in  $V_2O_3$  it is important to consider the underlying microscopic mechanism that leads to the transition. While it is well accepted that above  $T_c$  the electronic phase is metallic and below  $T_c$  it is a Mott insulator, the mechanism leading to the MIT cannot be described as a Mott transition. It is only recently, through a combination of neutron scattering measurements and first-principles calculations, that Leiner *et al.* convincingly demonstrated that it is instead a first-order phase transition between two states that host different magnetically ordered states in addition to being structurally and electronically distinct above and below the MIT  $T_c$  [3]. The metallic high-temperature (HT) phase was shown to be a strongly frustrated paramagnet, and the insulating low-temperature (LT) phase is a robust antiferromagnet with little frustration. Since the structural, electronic, and magnetic properties of  $V_2O_3$  are intimately linked, this makes the metal-insulator transition temperature sensitive to external perturbations.

Indeed, we have shown that the presence of point defects in the form of Frenkel pairs disrupts bonding and the magnetic ordering of the V atoms, which in turn leads to a reduction in

the energy to transition between the HT paramagnetic metallic phase and the LT antiferromagnetic insulating phase [5]. This is consistent with an experimental observation that found the MIT  $T_c$  to decrease when point defects are introduced intentionally compared to the  $T_c$  of as-grown  $V_2O_3$  [6]. The sensitivity of the MIT to changes in bonding has also made the use of strain an appealing approach to manipulate and control the MIT. This is part of a general growing interest in manipulating the transition temperature of materials that exhibit a MIT by taking advantage of advances in epitaxial growth, which has enabled the growth of thin films on targeted substrates [7].

Epitaxial growth of  $V_2O_3$  on *a*-plane (11 $\bar{2}$ 0), *c*-plane (0001), *m*-plane (1 $\bar{1}$ 00), and *r*-plane (1 $\bar{1}$ 02)  $Al_2O_3$  substrates has been explored by a number of groups [8–14]. Growth of  $V_2O_3$  on these substrates occurs at a temperature well above the MIT  $T_c$ , which results in a film that presumably adopts the HT paramagnetic corundum structure during growth. The  $Al_2O_3$  lattice constants are lower than the corundum  $V_2O_3$  lattice constants, so  $V_2O_3$  is expected to be under compressive strain if the growth is coherent. The reports of  $T_c$  identified from measurements of resistance versus temperature of these epitaxially grown films are varied. Schuler *et al.* demonstrated that the  $T_c$  increases by 45 K with respect to unstrained  $V_2O_3$  in a cooling cycle measurement of resistance versus temperature for  $V_2O_3$  grown on *c*-plane  $Al_2O_3$  [13]. In contrast, Kalcheim *et al.* [10] demonstrated that  $V_2O_3$  grown on the *m*-plane and *r*-plane orientations of  $Al_2O_3$  led to a  $T_c$  that is larger than the unstrained  $T_c$  (by up to 16 K), while growth on the *a*-plane orientation of  $Al_2O_3$  led to a reduction in  $T_c$ . Growth on alternative substrates, such as  $LiTaO_3$ , has also been explored where  $V_2O_3$  is expected to be under tensile strain if the growth is coherent [9,15,16]. In these studies, it was found that the  $T_c$  of  $V_2O_3$  was larger than the  $T_c$  of unstrained  $V_2O_3$ . An alternative approach to impart strain on  $V_2O_3$  has been through the use of ferroelectric and piezoelectric substrates that are subject to electrical biases with different polarity [17,18]. For instance, the  $T_c$  of  $V_2O_3$

\*Present address: Department of Physics and Astronomy, George Mason University, Fairfax, VA 22030, USA.

on a PMN-PT substrate increased by 30 K when the PMN-PT substrate underwent tensile expansion due to an applied bias.

The results of these experimental studies have been interpreted using the pressure versus temperature phase diagram of  $V_2O_3$  [1]. According to this phase diagram, positive pressure (volume reduction) leads to a reduction in  $T_c$  while negative pressure (volume expansion) leads to an increase in  $T_c$ . However, for a material under uniaxial or biaxial strain, the corresponding change in bonding can be very different from the change in bonding associated with hydrostatic pressure. Furthermore, first-principles calculations have demonstrated that relying on chemical pressure alone to interpret the  $V_2O_3$  phase diagram can be misleading [19]. To our knowledge, the impact of strain on the structural, magnetic, and electronic properties of  $V_2O_3$  has not yet been theoretically studied. Because of this, there is no clear relationship that can be deduced from the experimental reports on changes in the  $V_2O_3$   $T_c$  grown on different substrates and the magnitude and direction of the strain imparted.

In this study, we use first-principles calculations to investigate the effect of uniaxial and equibiaxial compressive and tensile strains on the structural, magnetic, and electronic properties of  $V_2O_3$ . We find that up to 1% compressive equibiaxial or uniaxial strains increase the energy required to transition to the LT antiferromagnetic insulating phase by up to 75% compared to unstrained  $V_2O_3$ . This would be reflected in an increase in the MIT  $T_c$  when  $V_2O_3$  is under compressive strain. In contrast, we find equibiaxial tensile or uniaxial tensile strains lead to modest reductions or increases in the energy to transition to the antiferromagnetic insulating phase depending on the direction along which the strain is imparted. We identify the microscopic origin of these changes in the energy to transition between the metallic and insulating phase as being changes in the bond lengths of the pair of next-nearest-neighbor vanadium atoms that are antiferromagnetically aligned in the LT monoclinic structure.

## II. COMPUTATIONAL METHODS

Our calculations are based on density functional theory within the projector-augmented wave method [20] as implemented in the VASP code [21,22] using the generalized gradient approximation defined by the Perdew-Burke-Ernzerhof (PBE) functional [23]. In our calculations, V  $4s^23p^63d^3$  electrons and O  $2s^22p^4$  electrons are treated as valence. All calculations use a plane-wave energy cutoff of 600 eV. Structural relaxations of the lattice parameters and internal coordinates were carried out with an  $8 \times 8 \times 8$   $k$ -point grid and a force convergence criterion of 5 meV/Å. To simulate the Mott-insulating behavior of  $V_2O_3$ , we use a spherically averaged Hubbard correction within the fully localized limit double-counting subtraction [24]. We apply a  $U$ - $J$  value of 1.8 eV to the V  $d$ -states, which reproduces the experimental band gap of  $V_2O_3$ . We note studies that compared exchange-coupling constants obtained from neutron scattering with first-principles calculations that relied on a larger value of  $U$ - $J$  (3 eV) to obtain quantitative agreement between theory and experiment [3]. We find our overall conclusions to remain unchanged if we also use a  $U$ - $J$  value of 3 eV.

To study the effects of epitaxial strain, we performed “strained-bulk” calculations where we impose compressive and tensile equibiaxial strain on the  $a$  and  $b$  (denoted as  $ab$ ),  $b$  and  $c$  (denoted as  $bc$ ), and  $a$  and  $c$  (denoted as  $ac$ ) monoclinic lattice vectors, and uniaxial strain along the  $a$ ,  $b$ , and  $c$  monoclinic lattice vectors of the  $V_2O_3$  unit cell, and then we optimize the free lattice constant(s) and all atomic positions of the unit cell. The standard VASP package does not allow for arbitrary constraints to be placed on the strain tensor during relaxation. To perform these constrained calculations, we made modifications that set specific components of the stress tensor to zero during the minimization routine. This allowed us to impose strain along the different axes as we report here.

Since growth of  $V_2O_3$  occurs at temperatures well above the MIT  $T_c$ , the as-deposited  $V_2O_3$  epitaxial films will adopt the HT paramagnetic structure. Paramagnetically ordered states are challenging to describe with standard DFT. However, since the paramagnetic HT phase is magnetically frustrated [3], magnetic ordering has a weak effect on total energies. We have previously shown that the FM ordered monoclinic structure can be used as a suitable proxy for the paramagnetic HT corundum phase [5]. Since strain is defined with respect to the HT phase, we use the lattice constants of the HT ferromagnetic structure as the reference for strain. For example, uniaxial strain along the monoclinic  $a$  axis,  $\epsilon_a$ , is defined as  $\epsilon_a = [(a - a_0)/a_0]$ , where  $a_0$  is the equilibrium  $a$  lattice constant of the FM monoclinic structure. In such a calculation, we would only allow the monoclinic  $b$  and  $c$  lattice constants, bond angles, and atomic coordinates to be optimized. Next, with this optimized structure we impose an AFM ordering of spins on the V atoms (ferromagnetic along the  $a$  and  $c$  axes and antiferromagnetic along the  $b$  axis), and we optimize the free lattice parameters and atomic coordinates. We report results for compressive and tensile strain along each of the monoclinic axes for strains that range between  $\pm 1\%$ . Positive values of  $\epsilon$  correspond to tensile strain.

## III. RESULTS

### A. Bulk properties

The HT metallic phase of  $V_2O_3$  is stable in the corundum structure with space group  $R\bar{3}c$ . Neutron scattering measurements in combination with first-principles calculations have demonstrated the corundum phase of  $V_2O_3$  to be a highly frustrated paramagnet [3]. As we discuss in Sec. II, we use a FM ordered structure as a proxy for the disordered paramagnetic phase of the corundum HT structure since it has the correct magnitude of the magnetic moments and it respects the full lattice symmetry (as opposed to an antiferromagnetic arrangement of spins). Indeed, we have previously shown that the energy difference between the corundum structure with FM order and AFM order imposed is low, 0.8 meV per vanadium atom [5], consistent with the magnetic frustration that has been experimentally identified in the HT phase [3]. Our DFT +  $U$  lattice constants of the FM corundum structure are  $a = b = 5.037$  Å and  $c = 14.305$  Å, and the bond angle of the rhombohedral unit cell is  $\theta = 54.6^\circ$ , which are within

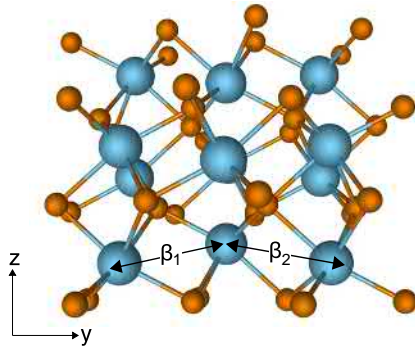


FIG. 1. Schematic illustration of the  $V_2O_3$  monoclinic unit cell. Vanadium atoms are in blue and oxygen atoms are in orange. The pair of V atoms that are antiferromagnetically aligned along the monoclinic  $b$  axis are denoted  $\beta_1$  and  $\beta_2$ .

1.5% of the experimentally measured lattice parameters of the HT corundum structure ( $a = b = 4.952 \text{ \AA}$ ,  $c = 14.003 \text{ \AA}$ , and  $\theta = 56.1^\circ$ ).

The LT insulating phase of  $V_2O_3$  is antiferromagnetic and has a monoclinic structure with space group  $P_21/c$ . We find the lattice constants of the LT monoclinic structure of  $V_2O_3$  to be  $a = 7.414 \text{ \AA}$ ,  $b = 5.084 \text{ \AA}$ , and  $c = 5.559 \text{ \AA}$ , and the bond angles to be  $\alpha = \gamma = 90^\circ$  and  $\beta = 97.3^\circ$ , which are within 2.7% of the experimental LT lattice parameters ( $a = 7.255 \text{ \AA}$ ,  $b = 5.002 \text{ \AA}$ ,  $c = 5.548 \text{ \AA}$ , and  $\beta = 96.8^\circ$ ) reported for monoclinic  $V_2O_3$  [25]. To describe the antiferromagnetic ordering of spins, we use a four-formula-unit cell. We find the ground-state magnetic ordering to be the one where the V atoms are aligned ferromagnetically along the monoclinic  $a$  and  $c$  axes and aligned antiferromagnetically along the monoclinic  $b$  axis, which is consistent with neutron scattering measurements of the monoclinic insulating phase [3,26].

Along the monoclinic  $b$ -axis, the pair of next-nearest-neighbor V atoms that are antiferromagnetically aligned have two different V-V bond lengths. We label the shorter of the two bonds  $\beta_1$ , and the second V-V pair is labeled  $\beta_2$ , as shown in Fig. 1. The bond length of the  $\beta_1$  pair is  $2.996 \text{ \AA}$ , while the bond length of the  $\beta_2$  pair is  $3.085 \text{ \AA}$ .

Since we are interested in the impact of strain on the energy to transition between the paramagnetic (approximated as ferromagnetic) HT phase and the antiferromagnetic LT phase using the “strained-bulk” approach, we also calculate the lattice parameters and electronic properties of the monoclinic structure where all of the V atoms are ferromagnetically aligned. If we allow for full structural relaxation (volume, cell shape, and atomic positions) in this magnetic state, we find that the structure takes on the HT corundum structure and is metallic.

## B. Biaxial and uniaxial strain

### 1. Structural properties

For the magnitudes of strain that we have investigated, we find that biaxial and uniaxial strain leads to elastic changes in the volume and in turn in the free lattice parameter(s). The monoclinic bond angle only changes by up to  $\pm 0.2\%$  for the largest strain ( $\pm 1\%$ ) that we consider.

If we consider biaxial strain imposed along the monoclinic  $ab$  axes, applying compressive equibiaxial strain to the FM structure and allowing the monoclinic  $c$  lattice parameter and all atomic positions to relax leads to an increase in the  $c$  lattice constant. We find that the  $c$  lattice constant increases linearly as a function of the applied compressive strain. Conversely, for equibiaxial tensile strain, the  $c$  lattice constant decreases linearly with respect to the  $c$  lattice constant of the unstrained FM structure. The ratio of the change in the  $c$  lattice constant as a function of the applied equibiaxial in-plane strain is a positive constant in the elastic regime and is defined as the Poisson ratio,  $\nu = -\epsilon_{zz}/(\epsilon_{xx} + \epsilon_{yy})$ , where  $\epsilon_{zz}$  is the strain in the  $c$  lattice constant, and  $\epsilon_{xx}$  and  $\epsilon_{yy}$  are the strains along the  $a$  and  $b$  monoclinic lattice constants, respectively. We find  $\nu = 0.31$  for the FM structure under equibiaxial strain along the  $ab$  axes. We find the response of the  $V_2O_3$  lattice to equibiaxial strain along the  $bc$  and  $ac$  axes to be similar; the free lattice parameter changes linearly with a Poisson ratio that is positive.  $\nu = 0.33$  for the FM structure under equibiaxial strain along  $bc$ , and  $\nu = 0.32$  for equibiaxial strain along  $ac$ .

Next we impose AFM ordering on the structures that are under equibiaxial or uniaxial tensile strain. As discussed in Sec. II, we assume that the lattice parameters of the HT paramagnetic (approximated as FM) would be clamped to the substrate post-growth and these lattice parameters remain fixed when the transition to the LT AFM insulating phase occurs. For example, for equibiaxial strain along the monoclinic  $ab$  axis,  $\epsilon_{ab}$ , of 1% (where  $\epsilon_{ab}$  is with respect to the equilibrium FM lattice parameters), we use the same monoclinic  $a$  and  $b$  lattice parameters that are strained by 1% with respect to the equilibrium FM monoclinic lattice constants, we impose AFM order, and we allow the monoclinic  $c$  lattice constant and all atomic coordinates to relax.

For each of the structures under strain with AFM order imposed, we find that the lattice also responds elastically with a positive Poisson ratio. The magnitude of  $\nu$  for the structures that are antiferromagnetically ordered for the different directions of equibiaxial strain are as follows:  $\nu = 0.36$  ( $ab$ ),  $0.38$  ( $bc$ ), and  $0.33$  ( $ac$ ).

### 2. Total energies

In Fig. 2, we illustrate the variation in the total energy of the FM and AFM configuration under biaxial strain along the monoclinic  $ab$  and  $bc$  axes and uniaxial strain along the monoclinic  $b$  axis. It is evident that the AFM configuration remains lower in energy than the FM configuration for all values of strain. For each of these values of strain, the FM configuration remains metallic while the AFM configuration remains insulating.

### 3. Spin-flip energies

From Fig. 2 it is also evident that the energy to transition between the high-temperature FM configuration and the low-temperature AFM configuration as a function of compressive and tensile strain is not a constant. For example, the total energy difference between the AFM and FM configuration under biaxial strain along  $ab$  is larger under compressive strain compared to tensile strain. We define this energy difference

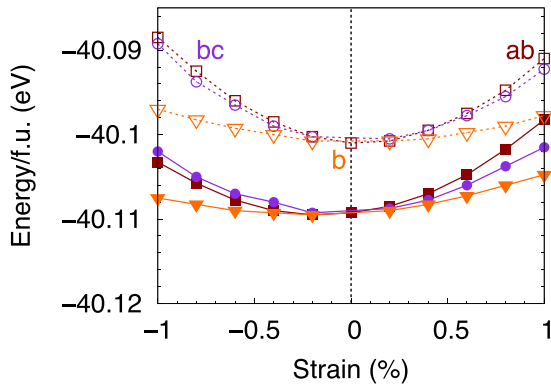


FIG. 2. Variation in the total energy of the AFM (solid line) and FM (dotted line) configuration per  $V_2O_3$  formula unit under compressive and tensile strain along the monoclinic  $ab$  ( $\square$ ),  $bc$  ( $\circ$ ), and  $b$  ( $\nabla$ ) axes. The vertical black dotted line denotes zero strain. Note, strain is defined with respect to the equilibrium lattice constants of the FM structure.

between the AFM and FM configuration at a fixed strain,  $\epsilon$ , a spin-flip energy,  $\Delta E$ , where  $\Delta E = [E_{\text{tot}}(\text{AFM}) - E_{\text{tot}}(\text{FM})]$ . Note that since the AFM configuration remains lower in energy than the FM configuration for all values ( $\pm 1\%$ ) and directions of strain that we consider in this study,  $\Delta E$  is always negative. An increase in the magnitude of  $\Delta E$  corresponds to an increase in the energy required to transition from the insulating AFM to the metallic paramagnetic (approximated as FM) state, while a reduction in the magnitude of  $\Delta E$  corresponds to a reduction in the energy to transition from the AFM to the FM state. The spin-flip energy as a function of equibiaxial and tensile strain is illustrated in Fig. 3.

We first consider the change in spin-flip energy for the structures subject to equibiaxial strain. Under compressive strain along the  $ab$  and  $bc$  axes, the magnitude of  $\Delta E$ , which is the energy required to transition from the insulating AFM state to the metallic FM state, increases by up to 75% at the largest value of  $\epsilon$  of 1%. Tensile strain along these axes

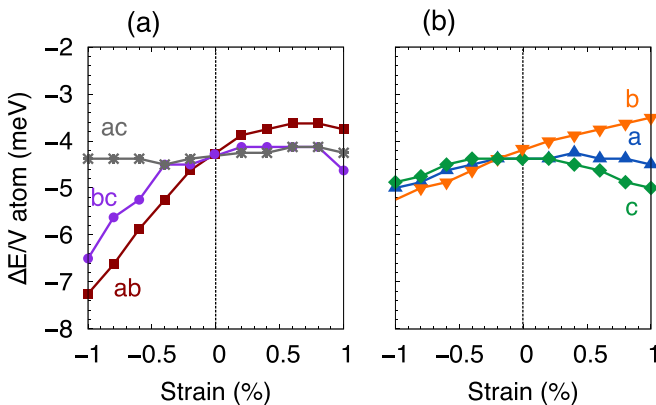


FIG. 3. Spin-flip energy,  $\Delta E = [E_{\text{tot}}(\text{AFM}) - E_{\text{tot}}(\text{FM})]$ , per V atom as a function of compressive and tensile (a) biaxial strain along the monoclinic  $ab$  ( $\square$ ),  $bc$  ( $\circ$ ), and  $ac$  ( $*$ ) axes, and (b) uniaxial strain along the monoclinic  $a$  ( $\Delta$ ),  $b$  ( $\nabla$ ), and  $c$  ( $\diamond$ ) axes. The vertical black dotted line denotes zero strain. Note, strain is defined with respect to the equilibrium lattice constants of the FM structure.

leads to a modest reduction in the magnitude of  $\Delta E$  for strain along  $ab$  and a modest increase in the magnitude of  $\Delta E$  for  $\epsilon$  greater than 0.5% along  $bc$ . In contrast, we find that  $\Delta E$  is insensitive to compressive and tensile equibiaxial strain along the monoclinic  $ac$  axes.

When  $V_2O_3$  is subject to uniaxial strain, we find the change in  $\Delta E$  to be modest in comparison to the change in  $\Delta E$  under biaxial strain. In particular, when the monoclinic  $a$ ,  $b$ , or  $c$  axes are under compressive strain, we find they all lead to a slight increase in the magnitude of  $\Delta E$ . Under tensile uniaxial strain, the magnitude of  $\Delta E$  increases for strain along the  $a$  and  $c$  axes, while the magnitude of  $\Delta E$  decreases for tensile strain along the  $b$  axis.

#### IV. DISCUSSION

At this point, it is instructive to examine the primary contributions to the change in  $\Delta E$  under compressive and tensile strain. We decompose this change in  $\Delta E$  into two contributions, namely an elastic energy,  $\Delta E^{\text{el}}$ , and a magnetic energy,  $\Delta E^{\text{mag}}$ , such that  $\Delta E = \Delta E^{\text{el}} + \Delta E^{\text{mag}}$ . The elastic energy,  $\Delta E^{\text{el}}$ , is the change in energy due to the change in the lattice parameters and the atomic positions to transition from the geometry associated with the FM to the AFM configuration at a fixed magnetic configuration. We define  $\Delta E^{\text{el}}$  as  $[E_{\text{tot}}^{[\epsilon, \text{FM}]}(\text{AFM}) - E_{\text{tot}}^{[\epsilon, \text{AFM}]}(\text{AFM})]$ , where  $E_{\text{tot}}^{[\epsilon, \text{FM}]}(\text{AFM})$  is the total energy of the structure with the atomic coordinates and lattice parameters of  $V_2O_3$  in the strained FM configuration with AFM order imposed, and  $E_{\text{tot}}^{[\epsilon, \text{AFM}]}(\text{AFM})$  is the total energy of the structure with the atomic coordinates and the lattice parameters in the strained AFM configuration and AFM order imposed. The magnetic energy,  $\Delta E^{\text{mag}}$ , is the change in energy associated with flipping spins from ferromagnetic to antiferromagnetic at a fixed set of atomic coordinates and lattice parameters. We define  $\Delta E^{\text{mag}}$  as  $[E_{\text{tot}}^{[\epsilon, \text{AFM}]}(\text{AFM}) - E_{\text{tot}}^{[\epsilon, \text{AFM}]}(\text{FM})]$ , where  $E_{\text{tot}}^{[\epsilon, \text{AFM}]}(\text{AFM})$  is the total energy of the structure with the atomic coordinates and lattice parameters of the strained AFM configuration with AFM order imposed, and  $E_{\text{tot}}^{[\epsilon, \text{AFM}]}(\text{FM})$  is the total energy of the structure with the atomic coordinates and lattice parameters of the strained AFM configuration with FM order imposed. For all values of biaxial and uniaxial strain,  $\Delta E^{\text{el}}$  only changes by up to 0.5 meV per vanadium atom. Note,  $\Delta E$  changes by up to  $\sim 4$  meV per vanadium atom in comparison to unstrained  $V_2O_3$  (Fig. 3). Hence, the remaining energy difference between  $\Delta E$  and  $\Delta E^{\text{el}}$  is the change in the magnetic energy,  $\Delta E^{\text{mag}}$ , as a function of strain.

Based on Fig. 3, it is evident that  $\Delta E$  is more sensitive to compressive strain in  $V_2O_3$ . To explain this sensitivity to compressive strain, we examine the bond lengths of  $V_2O_3$  in the AFM configuration. In the AFM configuration, the V atoms are ferromagnetically coordinated along the  $a$  and  $c$  axes and antiferromagnetically coordinated along the  $b$  axis. Previous first-principles calculations of the unstrained  $V_2O_3$  lattice [3] have demonstrated that the V atoms along the monoclinic  $b$  axis have the largest exchange coupling constants compared to the next-nearest-neighbor V-V exchange coupling constants along the other axes of the monoclinic structure. Within a nearest-neighbor Heisenberg model, the Néel temperature of the HT paramagnetic to the LT AFM phase transition would

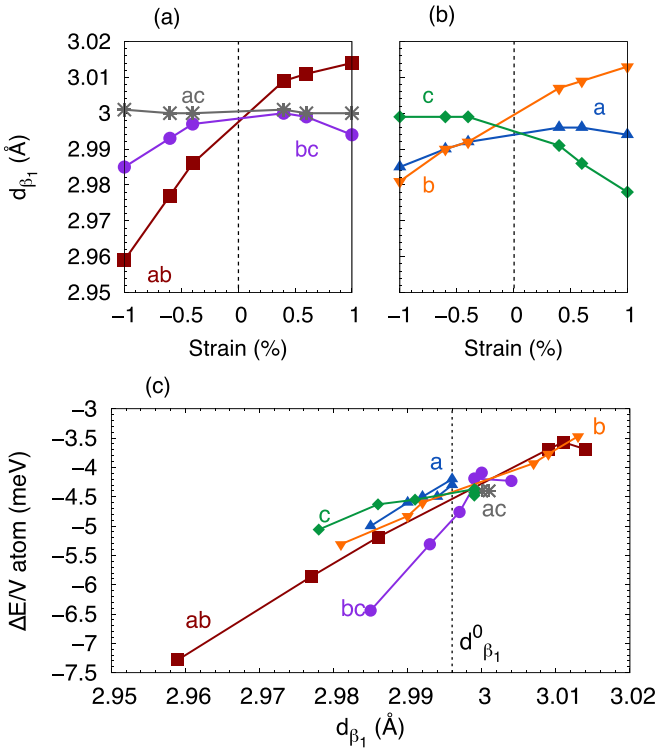


FIG. 4. Change in the bond length,  $d_{\beta_1}$  (cf.  $\beta_1$  in Fig. 1), as a function of compressive and tensile (a) biaxial strain along the monoclinic  $ab$  ( $\square$ ),  $bc$  ( $\circ$ ), and  $ac$  ( $*$ ) axes, and (b) uniaxial strain along the monoclinic  $a$  ( $\Delta$ ),  $b$  ( $\nabla$ ), and  $c$  ( $\diamond$ ) axes. The vertical black dotted line denotes zero strain. Note, strain is defined with respect to the equilibrium lattice constants of the FM structure. (c) Spin-flip energy vs change in the  $d_{\beta_1}$  bond length for the different directions of compressive and tensile strain imparted on the monoclinic axes. The  $d_{\beta_1}$  bond length of unstrained AFM  $V_2O_3$  ( $d_{\beta_1}^0 = 2.996$  Å) is shown with a dotted black line.

be determined primarily by the exchange coupling constants of these antiferromagnetically aligned V atoms. We denote these V-V bonds along the monoclinic  $b$  axis as  $\beta_1$  and  $\beta_2$  (Fig. 1), where the bond length of  $\beta_1$  ( $d_{\beta_1}$ ) is shorter than the bond length of  $\beta_2$  ( $d_{\beta_2}$ ). Leiner *et al.* [3] have shown that the exchange coupling constant of  $\beta_1$  is twice as large as that of  $\beta_2$ .

Through our first-principles calculations, we find that  $d_{\beta_1}$  changes nonmonotonically as a function of compressive and tensile strain. These results are illustrated in Figs. 4(a) and 4(b). Figure 4(c) illustrates the dependence of  $\Delta E$  on  $d_{\beta_1}$  for the different directions of strain we consider in our study. When  $d_{\beta_1}$  decreases with respect to  $d_{\beta_1}$  of the unstrained AFM monoclinic structure, we find that the magnitude of  $\Delta E$ , which is the energy to transition from the insulating AFM to the metallic FM state, increases, while an increase in  $d_{\beta_1}$  corresponds to a reduction in the magnitude of  $\Delta E$ . Since the primary contribution to the change in  $\Delta E$  is the magnetic energy, this dependence of  $\Delta E$  on  $d_{\beta_1}$  can be understood as follows. A reduction in the  $d_{\beta_1}$  bond length is expected to lead to an increase in the hopping energy,  $t$ , between the  $\beta_1$  pair of vanadium atoms (Fig. 1), which in turn would lead to an increase in the exchange coupling constant,  $J_{\beta_1}$ ,

where  $J_{\beta_1} \propto -t^2/U$ , and  $U$  is the on-site Coulomb repulsion. Conversely, we expect an increase in  $d_{\beta_1}$  to lead to a reduction in  $J_{\beta_1}$  compared to unstrained  $V_2O_3$ . This dependence of  $\Delta E$  on  $d_{\beta_1}$  also explains why equibiaxial compressive and tensile strain along the monoclinic  $ac$  axes does not lead to a change in  $\Delta E$ . We find that the biaxial strain that is imparted on the  $ac$  axes is accommodated by changes in  $d_{\beta_2}$  while  $d_{\beta_1}$  remains unchanged for all values of strain that we investigate [Fig. 4(a)].

Hence, our calculations suggest that the MIT  $T_c$  is sensitive to changes in the bond length,  $d_{\beta_1}$ . In particular, we suggest that compressive strain along the monoclinic  $bc$ ,  $ab$ ,  $a$ ,  $b$ , and  $c$  axes and tensile strain along the monoclinic  $bc$ ,  $a$ , and  $c$  axes will increase  $T_c$  compared to unstrained  $V_2O_3$ . We note that this is consistent with the increase in the MIT  $T_c$  that has been measured in  $V_2O_3$  thin films grown on  $Al_2O_3$  substrates, where  $V_2O_3$  is under compressive strain [8–10,13].

## V. SUMMARY AND CONCLUSIONS

In summary, we examined the role of equibiaxial and uniaxial compressive and tensile strain on the electronic, structural, and magnetic properties of  $V_2O_3$ .

The metal-insulator transition in  $V_2O_3$  was recently reinterpreted as being a strong first-order transition between the high-temperature corundum structure, which is a highly frustrated paramagnet, and the low-temperature monoclinic structure, which is strongly antiferromagnetic [3]. The leading contribution to the strong antiferromagnetic coupling in the low-temperature monoclinic phase is the shortest of the pair of V-V bonds that are antiferromagnetically aligned ( $\beta_1$ ) along the monoclinic  $b$  axis. As a result, shifts in the energy difference between the high-temperature metallic phase and the low-temperature insulating phase are sensitive to changes in the bond length of  $\beta_1$  of the LT AFM monoclinic phase. Our calculations confirm this interpretation and demonstrate that changes in the bond length of  $\beta_1$  due to strain can lead to changes in this energy difference. In particular, we find that a suppression of this energy difference, which would translate to a reduction in the MIT  $T_c$ , coincides with an elongation of the bond length of  $\beta_1$  while an increase of this energy difference coincides with a compression of the  $\beta_1$  bond length.

Based on our calculations, we can draw the following conclusions on the role of strain on the metal-insulator transition temperature of  $V_2O_3$ . Under compressive strain along the monoclinic  $bc$ ,  $ab$ ,  $b$ ,  $a$ , and  $c$  axes, the energy to transition to the low-temperature insulating antiferromagnetic phases increases by up to 75% for compressive strains up to 1%. Tensile strain along the monoclinic  $a$  and  $c$  axes leads to modest increases in the energy to transition to the insulating antiferromagnetic phase. Hence, strain along these directions and axes will likely lead to an increase in  $T_c$  compared to unstrained  $V_2O_3$ . Tensile strain along the  $ab$  and  $b$  axes lowers the energy to transition to the insulating phase by up to 10% compared to unstrained  $V_2O_3$  for the largest strain we consider of 1%, which would be reflected in a reduction in  $T_c$  compared to unstrained  $V_2O_3$ . In contrast, compressive and tensile strain along the monoclinic  $ac$  axes does not lead to any change in the energy to transition between the insulating and metallic phase.

## ACKNOWLEDGMENTS

We thank Ivan Schuller for helpful discussions and for encouraging us to undertake this work within the framework of the LUCI collaboration and Ivan Schuller's Vannevar Bush Faculty Fellowship program. D.W. acknowledges support

from the National Research Council fellowship at the U.S. Naval Research Laboratory. The work of N.B. and I.I.M. was supported by the Laboratory-University Collaboration Initiative (LUCI) of the Office of the Under Secretary of Defense for Research & Engineering Basic Research Office.

- 
- [1] T. M. Rice and D. McWhan, *IBM J. Res. Dev.* **14**, 251 (1970).
  - [2] L. Paolasini, C. Vettier, F. de Bergevin, F. Yakhou, D. Mannix, A. Stunault, W. Neubeck, M. Altarelli, M. Fabrizio, P. A. Metcalf, and J. M. Honig, *Phys. Rev. Lett.* **82**, 4719 (1999).
  - [3] J. C. Leiner, H. O. Jeschke, R. Valentí, S. Zhang, A. T. Savici, J. Y. Y. Lin, M. B. Stone, M. D. Lumsden, J. Hong, O. Delaire, W. Bao, and C. L. Broholm, *Phys. Rev. X* **9**, 011035 (2019).
  - [4] D. McWhan, A. Menth, J. Remeika, W. Brinkman, and T. M. Rice, *Phys. Rev. B* **7**, 1920 (1973).
  - [5] D. Wickramaratne, N. Bernstein, and I. I. Mazin, *Phys. Rev. B* **99**, 214103 (2019).
  - [6] J. G. Ramirez, T. Saerbeck, S. Wang, J. Trastoy, M. Malnou, J. Lesueur, J.-P. Crocombette, J. E. Villegas, and I. K. Schuller, *Phys. Rev. B* **91**, 205123 (2015).
  - [7] T. Saerbeck, J. de la Venta, S. Wang, J. G. Ramirez, M. Erekhinsky, I. Valmianski, and I. K. Schuller, *J. Mater. Res.* **29**, 2353 (2014).
  - [8] E. B. Thorsteinsson, S. Shayestehaminzadeh, and U. B. Arnalds, *Appl. Phys. Lett.* **112**, 161902 (2018).
  - [9] J. Brockman, M. Samant, K. Roche, and S. Parkin, *Appl. Phys. Lett.* **101**, 051606 (2012).
  - [10] Y. Kalcheim, N. Butakov, N. M. Vargas, M.-H. Lee, J. del Valle, J. Trastoy, P. Salev, J. Schuller, and I. K. Schuller, *Phys. Rev. Lett.* **122**, 057601 (2019).
  - [11] L. Dillemans, T. Smets, R. Lieten, M. Menghini, C.-Y. Su, and J.-P. Locquet, *Appl. Phys. Lett.* **104**, 071902 (2014).
  - [12] B. Allimi, S. Alpay, C. Xie, B. Wells, J. Budnick, and D. Pease, *Appl. Phys. Lett.* **92**, 202105 (2008).
  - [13] H. Schuler, S. Klimm, G. Weißmann, C. Renner, and S. Horn, *Thin Solid Films* **299**, 119 (1997).
  - [14] B. Sass, C. Tusche, W. Felsch, N. Quaas, A. Weismann, and M. Wenderoth, *J. Phys. Condens. Matter* **16**, 77 (2003).
  - [15] B. Allimi, M. Aindow, and S. Alpay, *Appl. Phys. Lett.* **93**, 112109 (2008).
  - [16] S. Yonezawa, Y. Muraoka, Y. Ueda, and Z. Hiroi, *Solid State Commun.* **129**, 245 (2004).
  - [17] P. Salev, J. del Valle, Y. Kalcheim, and I. K. Schuller, *Proc. Natl. Acad. Sci. USA* **116**, 8798 (2019).
  - [18] J. Sakai, M. Bavencoffe, B. Negulescu, P. Limelette, J. Wolfman, A. Tateyama, and H. Funakubo, *J. Appl. Phys.* **125**, 115102 (2019).
  - [19] F. Lechermann, N. Bernstein, I. I. Mazin, and R. Valentí, *Phys. Rev. Lett.* **121**, 106401 (2018).
  - [20] P. E. Blöchl, *Phys. Rev. B* **50**, 17953 (1994).
  - [21] G. Kresse and J. Hafner, *Phys. Rev. B* **47**, 558 (1993).
  - [22] G. Kresse and J. Furthmüller, *Phys. Rev. B* **54**, 11169 (1996).
  - [23] J. P. Perdew, K. Burke, and M. Ernzerhof, *Phys. Rev. Lett.* **77**, 3865 (1996).
  - [24] V. I. Anisimov, I. V. Solovyev, M. A. Korotin, M. T. Czyżyk, and G. A. Sawatzky, *Phys. Rev. B* **48**, 16929 (1993).
  - [25] P. Dernier and M. Marezio, *Phys. Rev. B* **2**, 3771 (1970).
  - [26] R. Moon, *Phys. Rev. Lett.* **25**, 527 (1970).